LAJSBA
LATIN AMERICAN JOURNAL OF SEDIMENTOLOGY AND BASIN ANALYSIS | VOLUME 30 (2) 2023, 163-184

RECENT DISTURBANCE EVENTS RECORDED IN THE SEDIMENTARY INFILL OF LAGO GUILLELMO (ARGENTINA): TEPHRA FALLS AND HYDROGEOMORPHIC PROCESSES

Pablo Amat [1], Gustavo Villarosa [1,2], Débora Beigt [1], Valeria Outes [1], Julieta Cottet [1,2], Lucía I. Dominguez [1], Alexander Cottescu [1], Andrés Barbosa [1]*

[1] Grupo de Estudios Ambientales (GEA-IPATEC, CONICET- UNCo), Av. de los Pioneros 2350, 8400, S. C. de Bariloche, Río Negro, Argentina.
[2] Centro Regional Universitario Bariloche, Universidad Nacional del Comahue, Quintral 1250, 8400, S. C. de Bariloche, Río Negro, Argentina.
* pabloamat@comahue-conicet.gob.ar

ARTICLE INFO

Article history
Received March 1, 2023
Accepted October 25, 2023
Available online November 11, 2023

Handling (guest) Editor
Alfonsina Tripaldi

Keywords
Disturbances
Lago Guillelmo
Lacustrine sedimentation
Tephras
Hyperpycnites

ABSTRACT

We studied two natural disturbances that affect the Parque Nacional Nahuel Huapi area: tephra fall events from Andean volcanoes and hydrogeomorphic processes within catchments related to heavy rains. We carried out a surface analysis, describing the main morphometric features of the selected watershed, informally called La Cantera watershed; analyzing satellite images and historical aerial photographs; looking for evidence of processes related to these disturbance events in the watershed and morphological changes in the alluvial fan generated over the delta. The subaqueous environment was analyzed through bathymetries, sediment cores, and Ground Penetrating Radar (GPR) profiles, taken in the distal deltaic environment of the watershed. In the sedimentary record of the lake, we identified 12 tephra layers deposited in the last 200 years, attributed to Cordón Caulle, Calbuco, and Osorno volcanoes. These were chronologically correlated with previously documented eruptions of these volcanic centers, using vitroclast morphology, mineral association, and stratigraphic position. We also identified 10 epiclastic layers corresponding to sediments with terrigenous components and terrestrial organic matter, interpreted as hyperpycnites. We assign two hyperpycnite deposits to a debris flow that occurred in the area in February 2015 that caused several damages and roadblocks, based on the stratigraphic position of these deposits in the cores, and the identification of sediments associated with this event on the lake surface in satellite images. After the correlation between the GPR radargram units with the lacustrine cores, we associated one major radar unit with a (1) tephra layer and (2) lobe-shaped morphologies, interpreted as a hyperpycnite deposits, located in front of the outflow of an abandoned river course. The results allow inferring a significant anthropic impact in the lacustrine record, as a result of the construction of Route 40 and gravel mining activities after 1969 that affected the distal drainage network of the La Cantera watershed, generating topographic lows that make it difficult for subaerial flows to reach the lake. This work shows the importance of the integration between subaerial processes that occur throughout a basin with the underwater processes that take place in the deltaic environment, to understand the extension and characteristics of these natural disturbances.

INTRODUCTION

The Nahuel Huapi region (Fig. 1a) is frequently affected by different disturbance events related to volcanic activity due to the proximity to the volcanoes within the Southern Volcanic Zone. The dominant westerly winds transport tephra plumes towards the Argentinian side of North Patagonia, causing several impacts in the region. In lacustrine environments, this pyroclastic material is deposited and preserved as discrete layers (Villarosa *et al.*, 2006; De Fontaine *et al.*, 2007; Bertrand *et al.*, 2014; Deng *et al.*, 2023). In watersheds, tephra deposits are prone to fluvial remobilization and are mostly redeposited in the lacustrine basins. Additionally, watersheds in the region are affected by disturbances related to hydrogeomorphic processes triggered by heavy rains (Chapron *et al.*, 2007). These rains frequently produce a hyperpycnal discharge that plunges freshwater and relatively light materials into the lakes. Originally transported materials within the fluvial discharge (*e.g.*, plant debris, trunks, charcoal) are forced to sink and to travel basinward within the hyperpycnal flow (Zavala *et al.*, 2018) giving rise to hyperpycnite deposits (Mulder *et al.*, 2003).

The study area is located in the southern area of Nahuel Huapi National Park (Río Negro, Argentina), in which paleoenvironmental reconstructions have been produced by several authors from a regional perspective. They identified tephra fall events, mass wasting deposits, and paleoenvironmental changes (Ariztegui *et al.,* 1997, 2001, 2008; Del Valle, 2000; Fontijn *et al.*, 2014, 2016; Alloway *et al.* 2022; among others), and reconstructed historical fires that affected the region (Mermoz *et al.*, 2005; Withlock *et al.*, 2006; Iglesias *et al.*, 2012; Iglesias and Whitlock, 2014). Mizerit (2017) evaluated the mass wasting susceptibility in the Guillelmo and Mascardi lakes, analyzing the control factors and main triggers of these processes. Cotello (2019) analyzed the risk of these events in the Lago Guillelmo region, along National Route 40, and proposed a mitigation plan. However, there is a lack of studies in the region that integrate the subaerial events and their corresponding signal or evidence in the lacustrine environment on a watershed scale. In this study, we aim to contribute to filling this gap, focusing our investigation on the La Cantera stream watershed and its postglacial fan delta and distal deltaic environment, located in the northwest portion of the Lago Guillelmo, Nahuel Huapi National Park. We perform a land surface analysis using morphometry description, historical and satellite images, with an original analysis of the subaqueous sedimentary environment, using bathymetries, lacustrine cores, and ground penetration radar (GPR) profiling, looking for evidence of these mentioned natural disturbances in the sedimentary record of Lago Guillelmo.

STUDY AREA

Lago Guillelmo (41°23'11" S; 71°29'39" W; 826 m a.s.l) has a glacial origin and is located at the eastern side of the Andean range (Northern Patagonia), 35 km south of San Carlos de Bariloche city and 2 km south of Villa Mascardi town (Fig. 1b). This lake has an estimated area of 5.4 km^2, 7.2 km of maximum length, and a maximum width of 1.8 km. The mean depth is 61.3 m, and the maximum depth is 107.2 m (Quiros, 1988). La Cantera watershed, in which the study zone is located (Fig. 1c), has temporary fluvial courses that flow into the lake through the postglacial fan delta that spreads over Lago Guillelmo (Fig. 1c). This watershed is also affected by the tracing of National Route 40, located next to the western portion of the lake.

Geologically, this area is located in the *Batolito Patagónico Cordillerano* (Gordon and Ort, 1993) composed of tonalites, granodiorites with hornblende and biotite, granite porphyries, and minor andesites intrusive bodies (Giacosa *et al.*, 2001). At least three glaciations affected this region during the Pleistocene (Flint and Fidalgo, 1964; Rabassa and Coronato, 2009) and nowadays it is possible to identify three major geomorphological units: watersheds and glacier-cryogenic relief, glacier valleys, and glacial erosional-depositional landscape (Pereyra *et al.*, 2009). This region is also affected by the volcanic activity associated with the Southern Volcanic Zone (SVZ), which results from the subduction of the oceanic Nazca plate under the South American plate (Stern *et al.*, 2004, 2007). In the study area, the most important volcanoes with documented activity during the Holocene are the Puyehue - Cordón Caulle Volcanic Complex (Lara *et al.*, 2006; Singer *et al.*, 2008; Alloway *et al.*, 2015, 2022), Osorno (Perez *et al.*, 2019) and Calbuco (Castruccio *et al.*, 2016; Romero *et al.*, 2021).

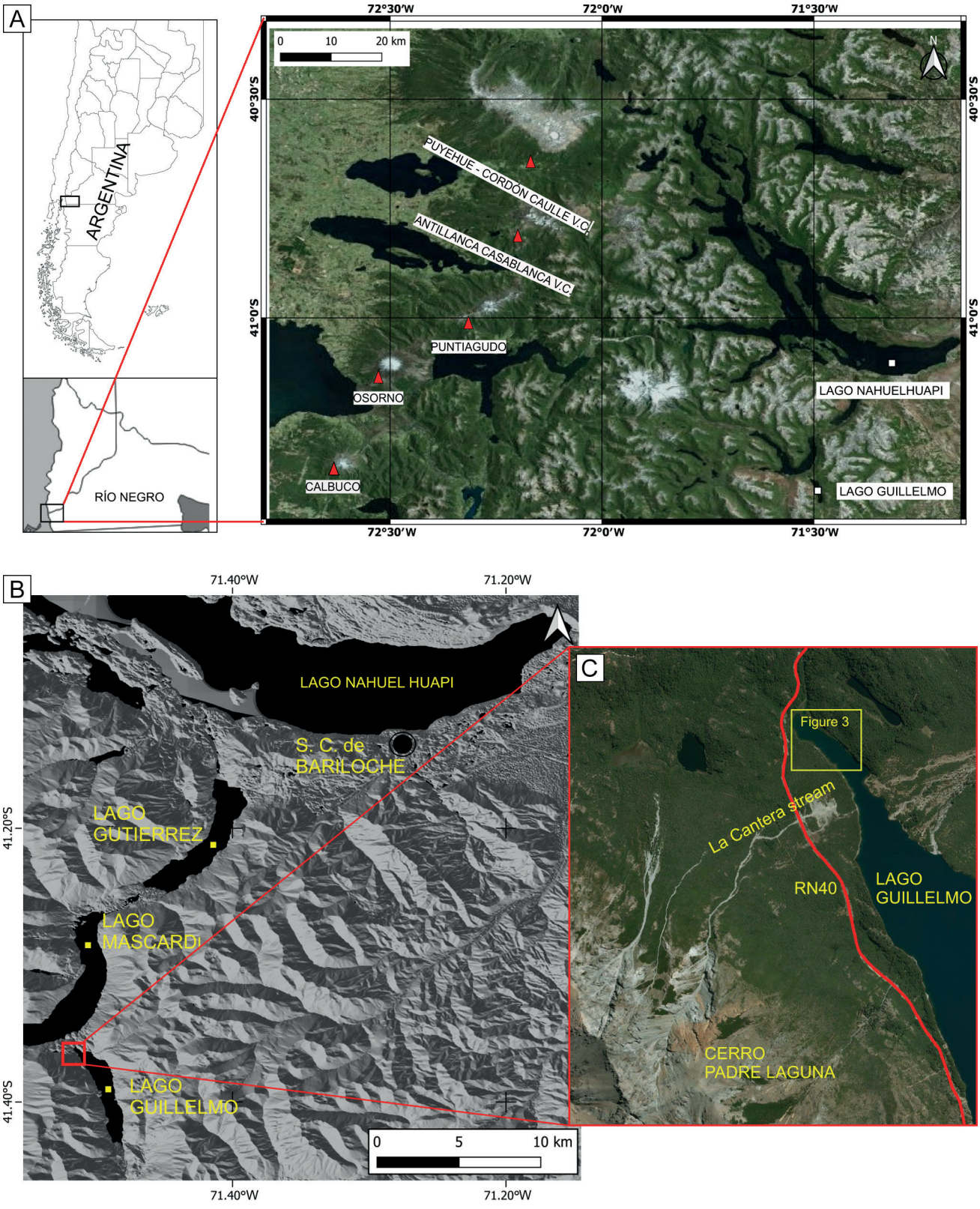

Figure 1. a) Study area (Lago Guillelmo) in relation to the active volcanoes of the region (Puyehue - Cordón Caulle V. C., Antillanca - Casablanca V. C., Puntiagudo, Osorno and Calbuco). **b)** Lago Guillelmo and nearby lakes (Mascardi, Gutierrez and Nahuel Huapi) and the coastal city of San Carlos de Bariloche. **c)** Detailed image of La Cantera stream and Lago Guillelmo. The yellow box in C corresponds to the location of Figure 3.

Northern Patagonia has a marked rainfall gradient in the West-East direction, the highest rainfall occurs in the Andes and gradually decreases eastward to the Patagonian Steppe. Mean annual precipitation decreases from 3000 mm in Andean rainforests to <500 mm only 80 km to the east (New *et al.*, 2002). This gradient causes a significant difference in vegetation. The study area is located in the Andean Patagonian Forest, Subantarctic Phytogeographic Province (Cabrera, 1976). The climate is temperate cool with an annual precipitation of 1500 mm and a mean annual temperature of 8.7ºC (Paruelo *et al.*, 1998). The concentration of rainfall occurs in the coldest semester (April-September), especially during May, June, July, and August (Pereyra *et al.*, 2009).

Recent disturbance events in the area

According to White and Pickett (1985), natural disturbance refers to any relatively discrete event in time that disrupts the ecosystem, community, or population structure and changes resources, or the physical environment. These disturbances include fires, insect outbreaks, disease epidemics, droughts, hurricanes, windstorms, landslides, avalanches, floods, and volcanic eruptions. There are several mentions of diverse types of disturbances in the study area, especially those related to mass removal processes and hydrogeomorphic processes, both in local and national newspapers such as El Cordillerano (2013), La Nación (2014), Telám Digital (2014), and Bariloche2000 (2015). These events vary from rockfalls to mud or debris flows and are associated with heavy rains during autumn and spring (Mizerit, 2017; Cotello, 2019; Mancini and Cordo, 2023). After each rain, large volumes of debris disrupt traffic at National Route 40 between the cities of San Carlos de Bariloche and El Bolsón, causing considerable disruption in land transport activities of the region. These events have become more frequent in the news since 2013, and one of the most important of them took place on February 2nd and 3rd 2015, when a debris flow advanced on the national route causing severe damage (Fig. 2) (Mancini and Cordo, 2023). According to the Sistema Nacional de Información Hídrica, during these days the daily precipitation varied from 11.1 to 35 mm, which are high values considering that, for the same weather station, the mean monthly precipitation in February was 42.4 mm in the period 1991-2020.

This region is also affected by pyroclastic fall events related to Andean volcanoes. Tephra layers were associated with the Puyehue-Cordón Caulle Volcanic Complex eruptions (Petit-Breuilh, 1995; Villarosa *et al.*, 2006; Chapron *et al.*, 2006; Bertrand *et al.*, 2014; Alloway *et al.*, 2015; among others). The activity of this volcanic complex started *ca*. 0.5 Ma ago with a wide range of compositions, evolving to mostly rhyodacitic and rhyolitic magmas in the Late Pleistocene-Holocene for both, the Puyehue Volcano and Cordón Caulle fissure system (Lara *et a*l., 2006; Singer *et al.*, 2008). Also, historical eruptions of the Calbuco Volcano were registered in this region by González-Ferrán (1995), Petit-Breuilh (1999), Daga *et al.*, (2014), and Romero *et al.*, (2016). The Calbuco Volcano has been active since the Pleistocene (~320 ka), with eruptive products ranging from basalts to dacites (50.5 to 64.5 wt% SiO_2) and historic products dominated by basaltic andesites and andesites (54.8–59.3 wt % SiO_2) (Romero *et al.*, 2021). Tephra layers from the Osorno Volcano were identified in the area by Petit Breuilh (1995) and Lara *et al.*, (2012). The Osorno Volcano is a Late Pleistocene to Recent composite stratovolcano that consists of aa-type lava flows interbedded with pyroclastic material.

METHODOLOGY

The methodology comprises land surface and subaqueous analyses using the characterization of the morphometry of the La Cantera watershed. Satellite and aerial images were analyzed looking for evidence of morphological changes due to the occurrence of hydrogeomorphic processes. Analysis of lacustrine cores and Ground Penetrating Radar (GPR) profiles were taken in the distal deltaic environment. Field surveys were carried out on the land surface and subaqueous environment.

Land surface analysis

La Cantera watershed was delimited using a Digital Elevation Model (DEM) with a spatial resolution of 5 m and submetric vertical accuracy provided by the Instituto Geográfico Nacional. Its basic morphometric parameters such as area (A), perimeter (P), length (L), mean width (W), maximum and minimum heights (H, h), and main channel length (Mcl), were quantitatively calculated using the open-

Figure 2. Debris flow event in La Cantera watershed that generated a roadblock on National Route 40 (3/2/2015). Source of the left image Digital Newspaper Bariloche 2000. Right image taken by the authors.

source software System for Automated Geoscientific Analyses (SAGA) v8.4.0 and QUANTUM GIS v.3.20.2. Several terrain profiles were generated to describe distal fan morphology. We also analyzed aerial photographs of 1969 and 1981, provided by Instituto Geográfico Nacional, and Google Earth Pro satellite images (2004-2019) for a preliminary assessment. Landsat 8 OLI/TIRS images, courtesy of the U.S. Geological Survey from the Google Earth Engine platform (Gorelick, 2017) of 2015-01-21 and 2015-02-06 for the same path and row, were used to identify changes in the fluvial network of La Cantera watershed and its fan delta. Fieldwork was conducted to identify sedimentary deposits related to tephra fall events and hydrogeomorphic processes in the area.

Subaqueous environment analysis

A bathymetric survey was conducted in the northwestern portion of the Lago Guillelmo to select the coring site using a dual-frequency echo sounder with GPS (Fig. 3). Using a modified UWITEC gravity-percussion sampler, we collected three short (<1 m) lacustrine cores, located about 30 meters from the coast and identified as GUI-1 (9.5 m depth; 41°21´47.76" S; 71°30'41.94" W), GUI-2 (9.3 m depth; 41°21'46.02" S; 71°30'45" W), and GUI-3 (5 m depth 41°21'39.60" S; 71°30'55.15" W) (Fig. 3). The sedimentology of the cores was described and analyzed using a digital X-ray imaging (Dinar AF-500 equipment) and magnetic susceptibility (MS) measurements on split-cores (Bartington M2SE) at 0.5 cm intervals. The sediment color was visually described using the Munsell Soil Colour Chart. GUI-1 was systematically subsampled at 1 cm increments to quantify the organic matter content by Loss on Ignition (LOI) at 105° and 550 °C (Bengtsson and Enell, 1986; Heiri *et al.*, 2001). Water content was calculated by weighting subsamples before and after drying at 105 °C. After the initial description of each core, we identified different layers, based on color, sediment grain size, clastic components, presence of volcanic glass, organic matter content and origin (lacustrine organic matter or terrestrial plant debris identification under stereomicroscope), sedimentary structure, magnetic susceptibility signal, and X-ray photographs. For tephra layer identification, we searched for intervals that correlate positively with MS fluctuations and negatively with water and organic matter content (LOI). These intervals can be traced by peaks in the MS profile and the other parameters (Guilizzoni *et al.*, 2009).

Several layers were subsampled for grain size analysis by sieving using mesh sizes 18, 35, 60, 120, and 230 (ASTM mesh numbers) and, in the specific case of tephra layers, to identify volcanic glass and petrographic components. These tephra samples were washed through a 63-μm sieve, cleaning the >63-μm fractions in a warm ultrasonic bath with distilled water to remove silt, clay, organic matter, and weathering products and drying them in a stove at 38 °C (Steen McIntyre, 1977). Then, samples were analyzed by stereomicroscope and compared with

tephras from eruptive centers that have affected this region, collected in lacustrine sediments, and stored at Laboratorio de Tefrocronología y Limnogeología (GEA-IPATEC). After the detailed description of these tephras, different vitroclast morphologies were associated with an eruptive style and magma type and therefore a volcanic center of origin (Heiken, 1974; Fisher and Schmincke, 2012; Romero *et al.,* 2016). We preliminary associate each tephra layer to a historically mentioned volcanic eruption, allowing estimation of the time span represented by the studied sedimentary record.

GPR is a geophysical method widely used in geology, although its application in aquatic environments for the study of lacustrine sediments is relatively new (Chanu *et al.*, 2014). The GPR system consists of a transmitter that emits high-frequency electromagnetic waves in the subsurface and a receiver that captures the energy reflected by its different layers. These layers present variations in their physical properties, according to their composition and water content. Factors affecting the maximum depth of penetration include the type of material, conductivity, and the frequency of the antenna used (Reynolds, 2011). In this study, GPR was employed to analyze the morphology and stratigraphic features of the lacustrine sediments.

The GPR system was GPS-synchronized, ensuring that the "x, y, z" coordinates were accurately linked to the GPR traces during profile acquisition. The system was placed on a boat, except for the 100 MHz Rough Terrain Antenna (RTA), which was positioned on the water surface, following Chanu *et al*. (2014). Three profiles (A-A', B-B', C-C') were conducted in the distal deltaic environment (Fig. 3). The radargrams were processed using the Rad Explorer software, which allowed the application of different filters to enhance the visualization of the radargrams and optimize their interpretation.

The applied filters included the Dewow filter, time-zero correction, pass-low filter, DC removal (direct current), BandPass filter, and amplitude correction with automatic gain control (AGC). The Dewow phase aims to eliminate low-frequency and DC bias in the data. Time-zero correction corrects the initial time of the first peak to be the same as the surface of the ground. The DC Removal routine removes the constant component of the signal if present. The "Bandpass Filtering" routine is used to increase the signal-to-noise ratio. The "Amplitude correction" routine aims to enhance the signal that has propagated deeper by multiplying the signal with a certain amplification factor so that it can be seen or read (Maruddani and Sandi, 2019). With the electromagnetic wave velocity and the relative dielectric constant of the medium, it is possible to compute the thickness of the reflectors visible in the radargram (Reynolds 2011, p. 539 - 551). With these parameters in hand and employing Rad Explorer, we managed to determine the thickness of the initial reflectors and, consequently, correlate them with the units observed in the cores (GUI-1, GUI-2, and GUI-3).

RESULTS

Description and morphometry of the La Cantera watershed

The area of this watershed is 1.662 km^2 and its perimeter is 7.529 km. The main width is 0.28 km and its total length is 2.734 km. The main stream of this watershed (La Cantera stream) flows along the eastern flank of Cerro Padre Laguna down to its fan delta that spreads over Lago Guillelmo. The maximum height is 1867 m a.s.l and the minimum height is 819 (Fig. 4).

Satellite images and aerial photographs analysis. After comparing different satellite and historical images, three different fluvial courses (C1, C2, and C3) were identified in the aerial photograph of 1969, where C1 was the most active, and the alluvial fan before the construction of the National Route 40 was also clear. In this image, the alluvial fan is covered with vegetation and we identified that C2 outflow corresponds to the location of the GUI-2 coring site (Fig. 5a). In the aerial photograph of 1980, anthropic activity in the distal zone of the watershed, associated with the construction of the National Route 40 and a gravel mining pit, is evident. There is a lack of official data on the gravel mine establishment, but it seems the main objective was to provide the material (sand and gravel) for the National Route 40 construction (Vialidad Nacional, personal communication). By the 1980s, C1 was channeled beneath the route. In this image, C1 is still the most active channel, while C2 and C3 begin to lose importance (Fig. 5b). During 2013, C1 was the only fluvial course that showed activity, and C2 and C3 were completely abandoned

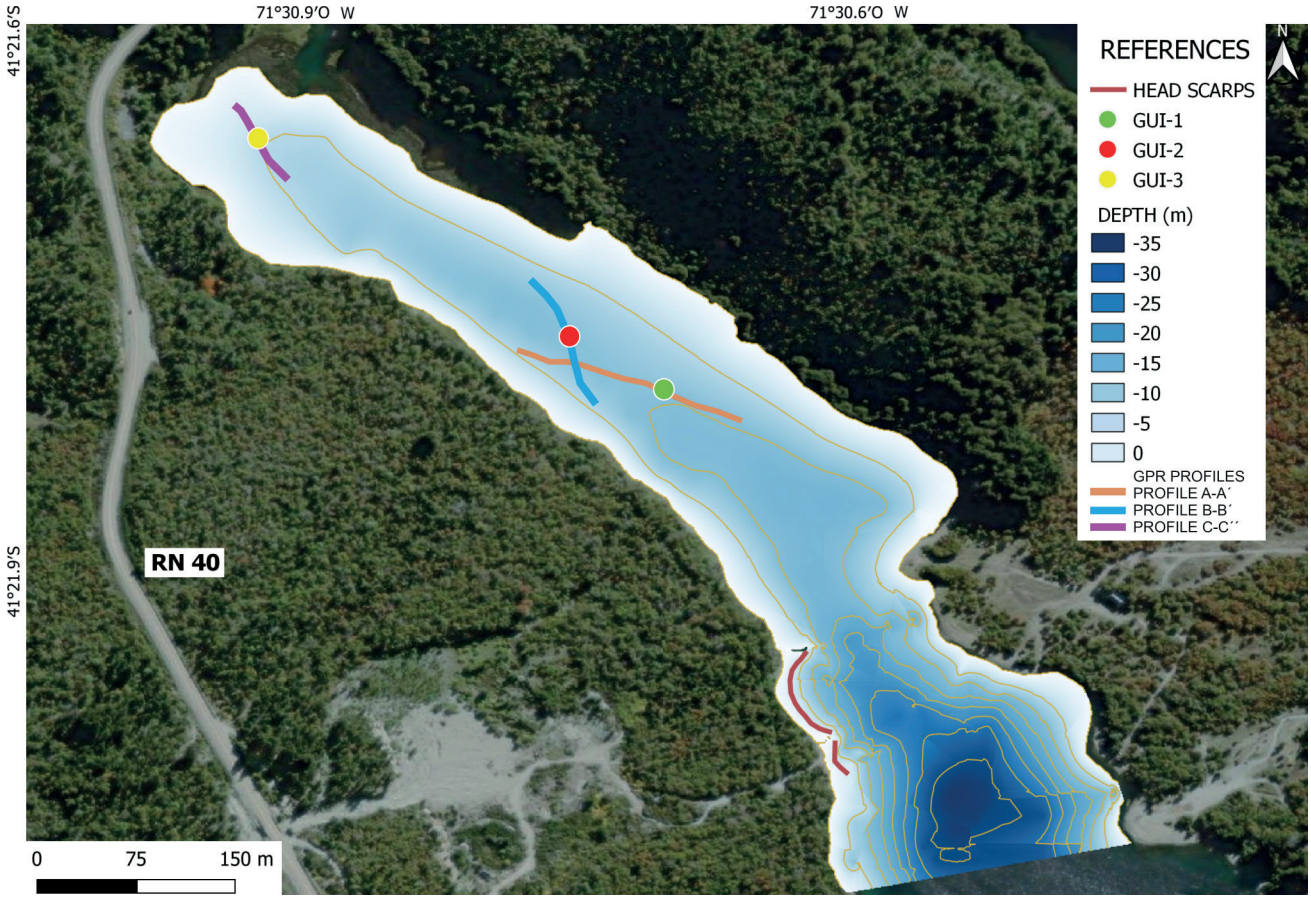

Figure 3. Bathymetric map of Guillelmo lake and coring sites and GPR profiling location.

(Fig. 5c). In the 2016 Google Earth image (Fig. 5d), a hydrogeomorphic event was identified: probably a debris flow that overflowed the abandoned courses of C2 and C3 and reached the distal zone of the alluvial fan.

After the initial comparison between Google Earth images of 2013 and 2016 (Fig. 5 e-f), and the detailed analysis of the Landsat 8 OLI/TIRS images of 2015 (Fig. 5 g-h), we linked this event to a debris flow that took place during February 2nd and 3rd 2015 in this area, and was mentioned by Mancini and Cordo (2023) and local newspapers. Sediments in the lake surface were also identified in these images, showing that the debris flow reached the lacustrine environment, marked by a shift in the hue of the water from dark to light blue as a result of an increase in water reflectance. Similar phenomena were noted in glacial lakes by Beigt *et al.* (2023), Giardino *et al.* (2010), and Matta *et al.* (2017). During fieldwork, sedimentary deposits associated with this event were identified showing massive and partially inversed graded, massive matrix-supported cobbles to pebbles (Fig. 5i). In addition, we observed low topographies or depressed areas associated with the material extraction in the mine pit area in the distal part of the stream.

Bathymetric analysis

The bathymetry shows that the maximum depth of this sector is 32 m. At least three head scarps associated with subaqueous landslides were identified near the outflow of La Cantera stream into the lake. Subaqueous morphologies and stratigraphic mass wasting features in northern Patagonian lakes were recognized by Chapron *et al.* (2006) and Villarosa *et al.*, (2009). Beigt *et al.*, (2023 and references therein), demonstrated that these processes are much more frequent in deltaic environments due to steep delta fronts and high sedimentary rates. The coring sites were located away from these head scarps, in the undisturbed prodelta environment located at the northern portion of the lake, dominated by poorly disturbed sediments.

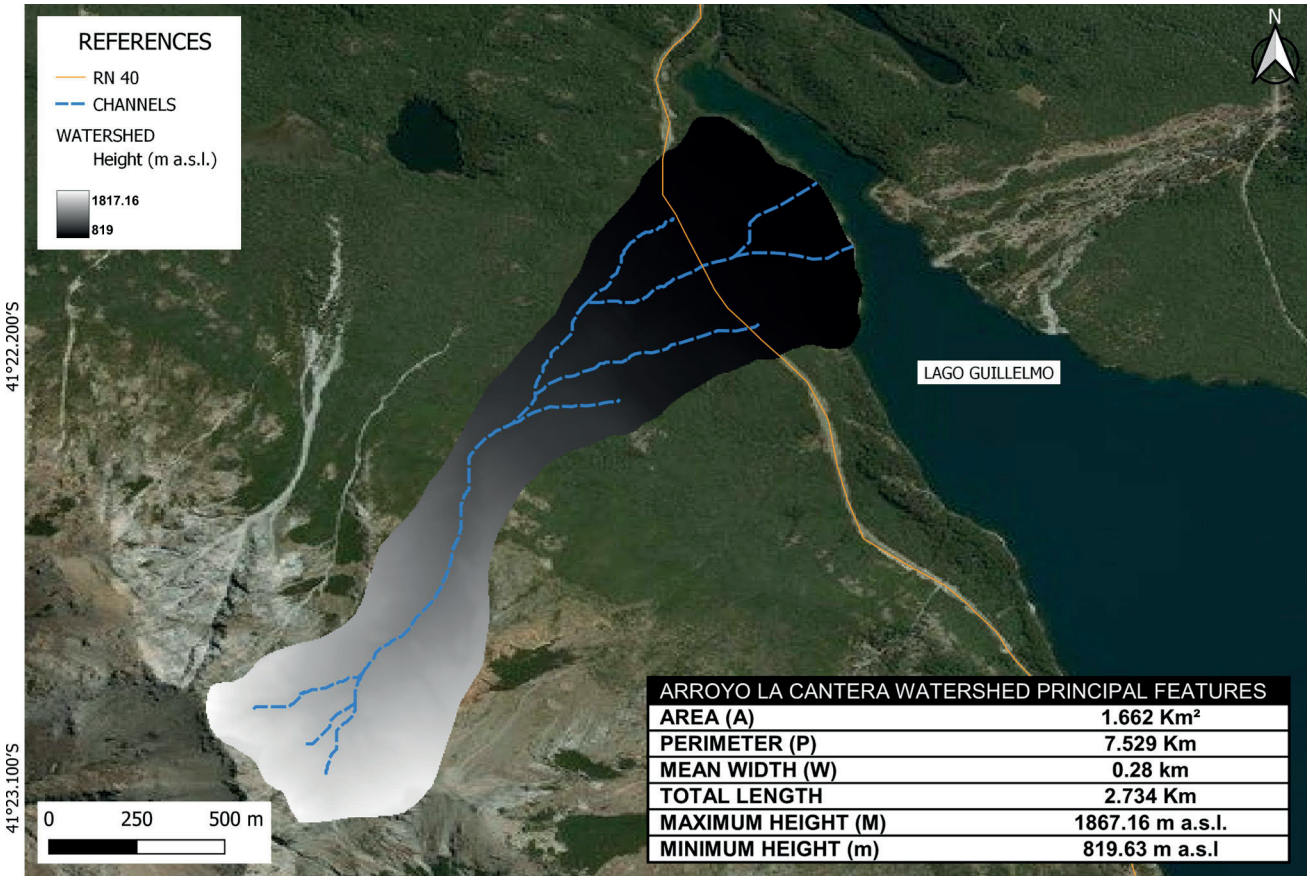

Figure 4. Delimitation and principal morphometric features of La Cantera watershed.

Cores description

Core GUI-1. Two lithological units were identified in the 77.5 cm-long GUI-1 core: a basal unit of medium gray, laminated coarse silt to very fine sand below 9.8 cm depth (Unit 1; Fig. 6), overlain by moderate yellowish brown, massive, organic-rich sediments (Unit 2; Fig. 6). Although the sediment lamination is visually diffuse, it is clearly defined in the XR image (Fig. 6). A thick tephra layer (L5) at 10.2–9.8 cm depth was evidenced by high magnetic susceptibility and five coarse epiclastic sediment layers (L1, L2, L3, L4, and L6) with terrestrial plant debris were noted by visual observation (Table 1). The basal unit is characterized by low values of organic matter (2-10 %) and variable water content (29-59 %) with high magnetic susceptibility values, consistent with abundant increased allochthonous input into the lake. The lithologic change was registered by a gradual increase in organic matter (10-14%) and water content (59-69%) coupled with low values of magnetic susceptibility in the sediment, suggesting an increase in lake productivity.

Core GUI-2. Three lithological units were identified in the 47 cm-long GUI-2 core (Fig. 7). The basal unit (Unit 1, 47-37 cm depth) corresponds to an olive gray discrete laminated, normally graded sand layer (from medium sand to very fine sand), with a 4 mm layer of gray clay on top of it. This unit stands out due to its thickness (9 cm) and notorious presence of terrestrial plant debris (roots, leaves, charcoal), easily recognized under a stereomicroscope (Fig. 8 a-b). The second unit (Unit 2, 37-10 cm) corresponds to brownish-gray, diffusely laminated coarse silt to very fine sand. Lamination is well noted in the XR image (Fig. 7). Unit 2 is overlain by massive, brownish-gray to dark brown organic-rich sediments (Unit 3, 10 cm-0 cm depth) with an 8 mm layer of gray fine sand on top of it. Lacustrine organic matter, corresponding with macro remains of charophytes, similar to those described by Soulié-Märsche and García (2015), were identified in Units 2 and 3. Five epiclastic accumulations (L1, L2, L3, L4 and L6) and

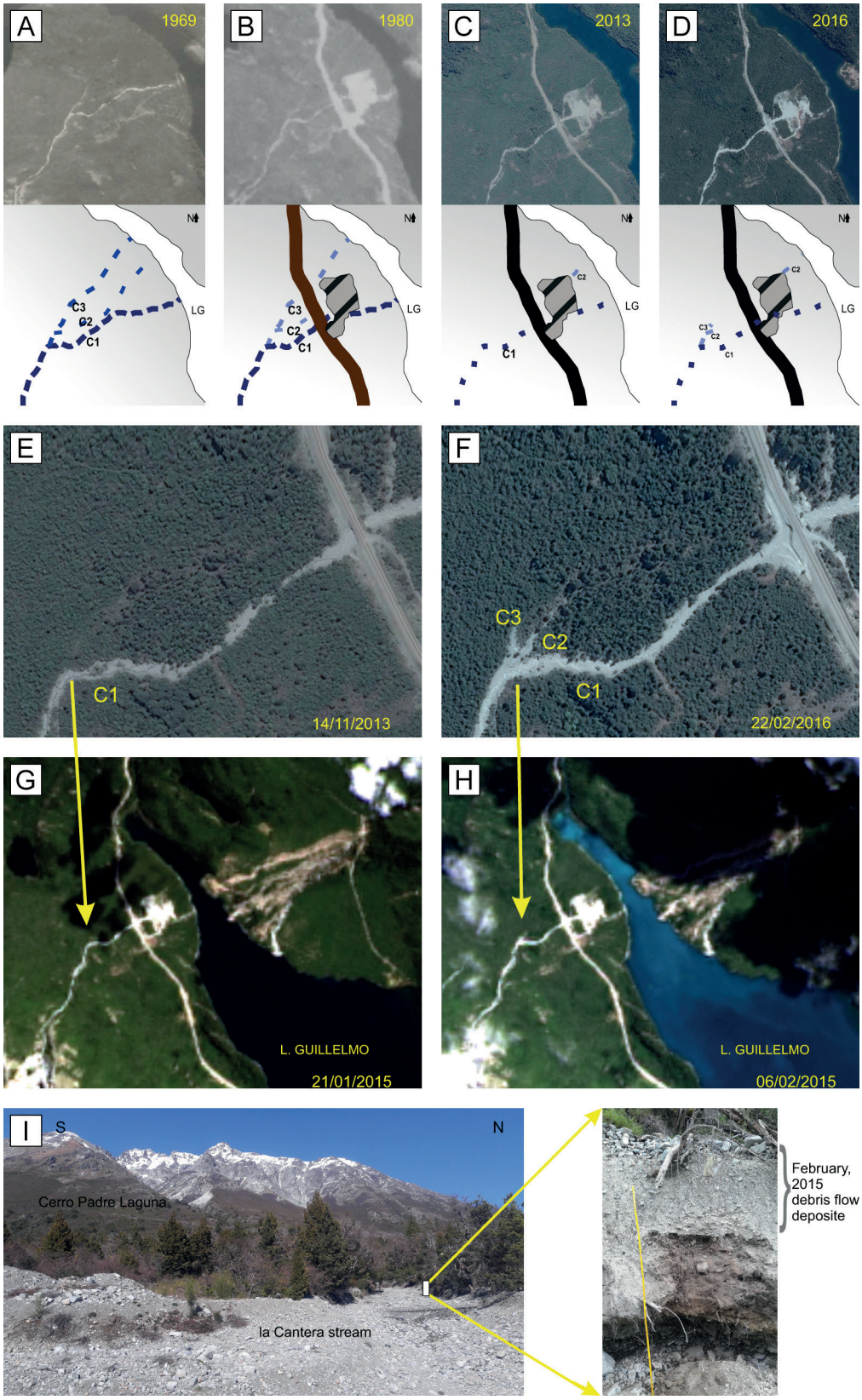

Figure 5. a, b, c and **d)**Time series and interpretation of streams in relation to mine pit. **e)** Google Earth images of 2013. **f)** Google Earth Image of 2016 showing the debris flow over the C2 and C3 abandoned courses. **g)** Landsat 8 OLI/TIRS true color (RGB: 4-3-2) of 21/01/2015. **h)** Landsat 8 OLI/TIRS true color (RGB: 4-3-2) of 06/02/2015, light blue color in the lake shows the presence of suspended sediments in the water. **i)** Deposit of February 2015 debris flows recognized near to the intersection between the National Route 40 and La Cantera principal stream (C1).

GUI-3				GUI-2				GUI-1			
CODE	DEPTH (cm)	THICKNESS (cm)	MAIN CHARACTERISTICS	CODE	DEPTH (cm)	THICKNESS (cm)	MAIN CHARACTERISTICS	CODE	DEPTH (cm)	THICKNESS (cm)	MAIN CHARACTERISTICS
L10	7.5 - 7.2	0.3	Tephra – Two vitroclast populations: (1) Pumiceous light brown to greenish brown vitroclast, and (2) scoriaceous vitroclast. Presence of plagioclase, pyroxene, and scarceolivine.	L 6	1 - 0.2	0.8	Sandy siltlayer, clastic terrigenous components, scarce presence of terrestrial plant debris.	L 6	1 – 0.2	0.8	Sandy siltlayer, clastic terrigenous components, scarce presence of terrestrial plant debris.
L9	25.7-25.5	0.2	Tephra – Two vitroclast populations: (1) Pumiceous light brown to greenish brown vitroclast, and (2) scoriaceous vitroclast. Presence of plagioclase, pyroxene, and scarce olive.	L 5	9.5 -8.5	1	Tephra – two vitroclast populations: pumiceous light brown to greenish brown vitroclasts, and scoriaceous vitroclasts. Presence of plagioclase, pyroxene, and scarceolivine.	L 5	10.2-9.8	0.4	Tephralayer – twovitroclastpopulations: (1) Pumiceous light brown to greenishbrownvitroclasts, and (2) scoriaceous vitroclasts. Presence of plagioclase, pyroxene, and scarceolivine.
L8	46.5 - 45.9	0.6	Tephra – Three major vitroclast populations: (1) White to lightly coloured pumiceous elongated fragments (2) Brownish pumiceous highly vesiculated fragments, (3) dark gray scoriaceous fragments. Presence of plagioclase and scarceolivine.	L 4	15 - 14	1	Fine sandlayer, epiclastic components (grains of quartz, lithic fragments), presence of terrestrial plant debris.	L 4	20.9 – 20.1	0.8	Fine sand layer, epiclastic components (grains of minerals, lithic fragments), presence of terrestrial plant debris
L7	48.3 - 48	0.3	Tephra – Two major vitroclast populations: (1) White to lightly coloured pumiceous fragments (2) Dark gray scoriaceous fragments. Obsidian fragments. Presence of pyroxene and possibly olivine.	L 3	17 - 15.5	1.5		L 3	22.3 –21.6	0.7	
L6	51 - 50	≈ 0.2	Tephra – Two major vitroclast populations: (1) White to lightly coloured pumiceous fragments (2) Dark gray scoriaceous fragments. Presence of plagioclase, pyroxene.	L 2	31.5 - 30	1.5		L 2	37.9 – 36.1	1.8	
L5	55.1 - 55	0.1	Tephra – A major population of dark scoriaceous vitroclasts. Presence of plagioclase, pyroxene, and possibly olivine.	L 1	47 - 38.5	8	Up grading, medium sand to very fine sand with a 4 mm of clay on top, poorly laminated at the top, presence of terrestrial plant debris	L 1	74.1 – 72.9	1.2	

Table 1. Continued on page 173.

GUI-3			
CODE	DEPTH (cm)	THICKNESS (cm)	MAIN CHARACTERISTICS
L4	≈ 56,5	0.5 - 10	Tephra – Two major vitroclast populations: (1) White to lightly coloured pumiceous fragments (2) Scarce dark gray scoriaceous fragments. Presence of plagioclase, pyroxene and scarce hornblende.
L3	73.1 - 72.9	0.3	Tephra – two major vitroclast populations: (1) White to light-coloured pumiceous fragments (2) Dark scoriaceous fragments. Obsidian fragments. Presence of pyroxene, and possiblyolivine.
L2	76.4 - 75	0.4	Tephra – two major vitroclast populations: (1) White to lightly coloured pumiceous fragments (2) Dark gray scoriaceous fragments. Presence of plagioclase, pyroxene.
L1	81 - 79.5	1.5	Tephra – two vitroclast populations: (1) Dark gray to black scoriaceous fragments, with scarce vesicularity (2) Greenish broken droplets, with flat surfaces and vesicularity. Presence of quartz, plagioclase, and scarceolivine.

Table 1. Layers of interest identified in GUI-1, GUI-2 and GUI-3 cores and their main characteristics.

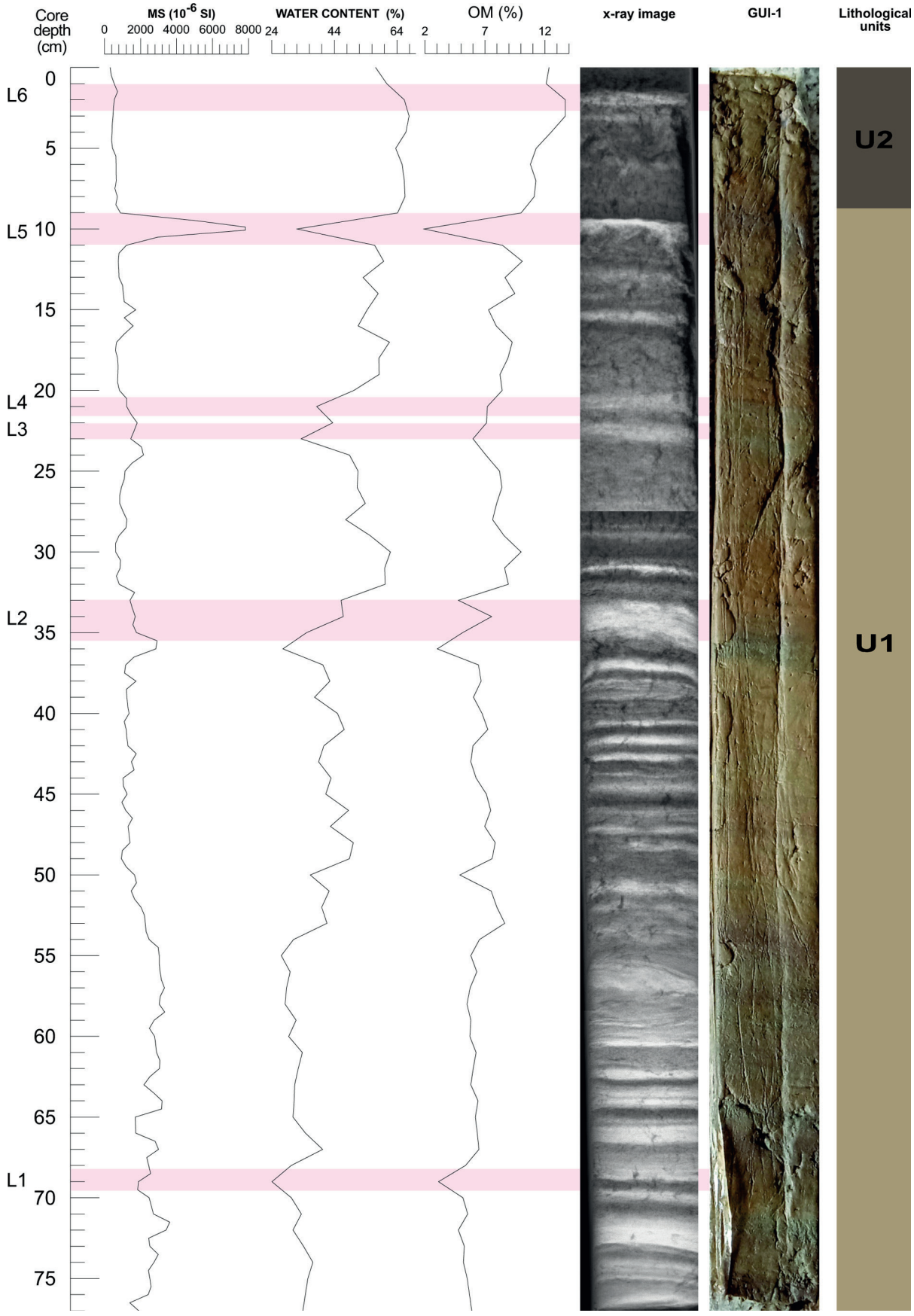

Figure 6. Magnetic susceptibility, water content, organic matter, X-ray image and photograph of GUI–1 core. The pink shaded areas indicate the intervals where the layers of interest are located.

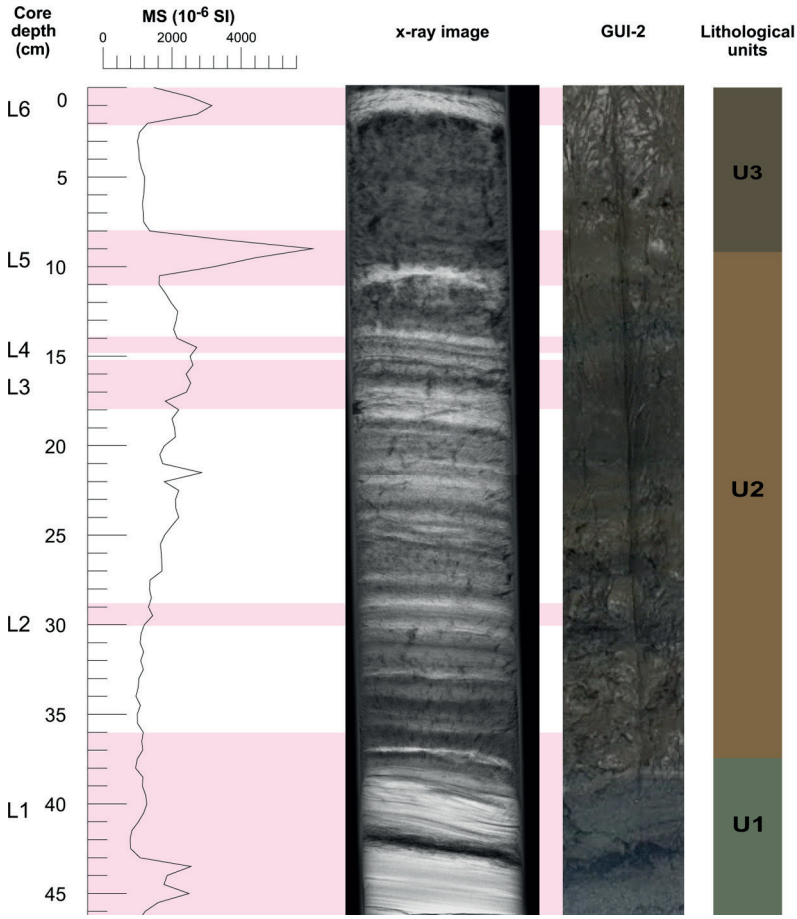

Figure 7. Magnetic susceptibility and X-ray image of GUI-2 core. The pink shadows indicate the intervals where the layers of interest are located.

one tephra layer (L5) were identified (Table 1). L1 corresponds to Unit 1, L2, L3, L4, and L5 are located in Unit 2, finally, L6 is on top of Unit 3.

Core GUI-3. The 83.5 cm-long GUI-3 core is divided into two lithological units (Fig. 9): a basal section of olive-gray, diffusely laminated coarse silt to very fine sand (Unit 1, 83.5-16 cm depth), overlain by massive moderate yellowish brown organic-rich sediments (Unit 2, 16-0 cm depth). The lamination is diffuse both macroscopically and in the XR image. Ten tephra layers (L1 to L10, Table 1) were initially identified by MS peaks, later confirmed by petrographic observations.

Broken droplets with flat surfaces and scoriaceous fragments were identified in L1 (Fig. 10a-c). In L3, L4, and L8 we recognized white to light-colored, highly vesicular pumiceous fragments, (Fig. 10d-f) and obsidian fragments (Fig. 10g-i). In L2, L5, L6, L7, L9, and L10 dark scoriaceous and pumiceous fragments were observed (Fig. 10j-l).

GPR analysis

The system's resolution (100 MHz antenna) was such that it allowed the identification of individual units within the sediment. Three radargrams were acquired, each displaying well-defined reflectors. Various significant reflectors were identified, corresponding to the interfaces between layers with distinct electromagnetic properties, associated with sediment characteristics (Van Dam *et al.*, 2003). In this work, the set of significant reflectors that present consistency from the stratigraphic and morphological point of view is defined as a radar unit. For profile A-A' (Fig. 11), a radar unit was identified at approximately 50 cm depth, which could correspond to the set of tephra layers L3, L4, L5, and L6 from core GUI-3, located at 50 - 73 cm depth.

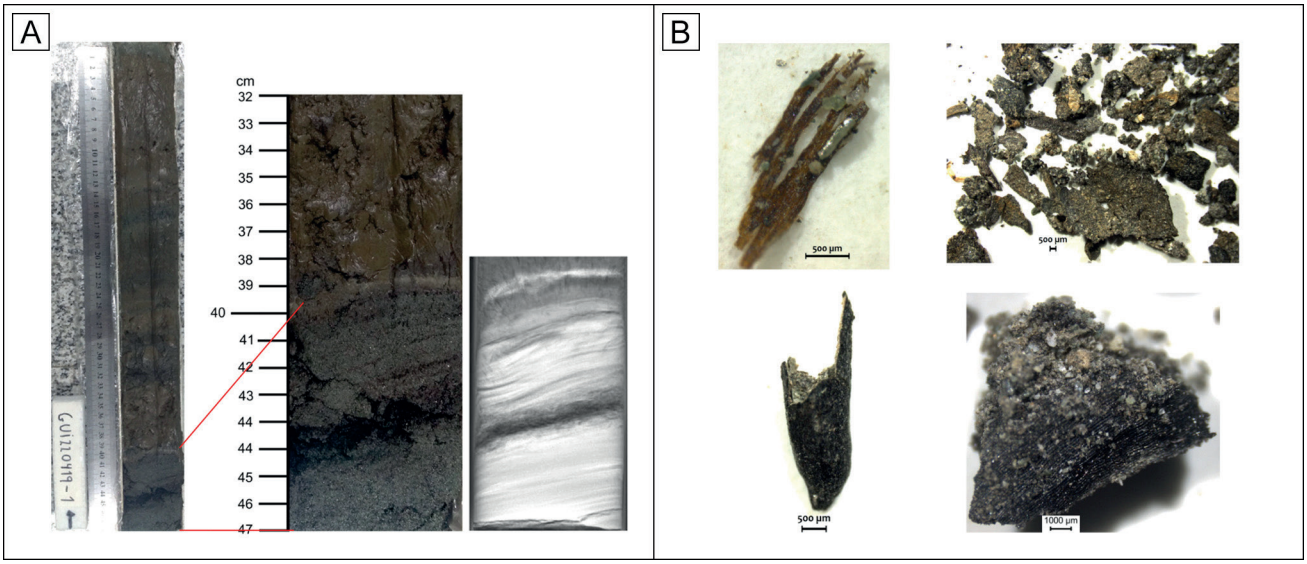

Figure 8. a) L1 – GUI-2 layer of interest. **b)** Terrestrial plant debris identified in this L1.

For profiles B-B' and C-C' (Fig. 11), a very faint initial reflector was observed, which could represent the water-sediment interface, followed by a radar unit which may correspond to the background sediment. At approximately 42 cm depth (Fig. 11), a radar unit with lobulated morphology would correspond to the L1 layer of core GUI-2.

DISCUSSION

The lake deposits are characterized by the presence of epiclastic and pyroclastic material mixed with autochthonous sediments derived from the local productivity of the lake. In this sedimentary succession, it is possible to distinguish two types of episodic sedimentation: pyroclastic falls and hyperpycnal flows. Figure 12 summarizes the findings on the three cores.

Pyroclastic fall events reconstruction

As mentioned above, the study area is influenced by the volcanic activity of SVZ. Due to the proximity to these volcanoes and dominant westerly winds, there is an eastward transport of tephras to the North Patagonia area. A preliminary correlation between volcanic products deposited in the region and the tephra layers identified at Lago Guillelmo allowed us to associate these layers with Cordón Caulle, Calbuco, and Osorno volcanoes.

A tephra composed of broken droplets and scoriaceous fragments (L1; GUI 3; 81 - 79.5 cm depth) was associated with basaltic magmas (48-52% SiO_2) following Heicken (1974). According to this interpretation, we consider that this tephra corresponds to the Osorno Volcano. The effusive products of this volcanic center are mainly aphyric and porphyritic basalts and basaltic andesites, where plagioclase is the most abundant phenocryst phase followed by olivine and clinopyroxene (López-Escobar *et al.*, 1992). In Lake Puyehue, Bertrand *et al.*, (2008) describe an Osorno basaltic andesite tephra level composed of opaque to partly translucent scoriae, brownish glass shards, and crystals (olivine, orthopyroxene, and clinopyroxene). L1 was attributed to the 1835 Osorno eruption, characterized by a volcanic explosivity index (VEI) 3 (Petit Breuilh, 1995; Lara *et al.*, 2012; Global Volcanism Program, 2023). There are reports of minor fumarolic and weak explosions of this volcano after the 1835 eruption, but due to the thickness of the layer (1.5 mm), we infer that this tephra corresponds to the 1835 event. Considering that this layer is located near the bottom of the GUI-3 core, we estimate that this sedimentary record spans the last 190 years.

The subsequent tephra layers of GUI-3 core (L2, L4, L6, L9, and L10), composed of both brownish and greenish pumice fragments and scoriaceous fragments, were associated with basaltic-andesitic to andesitic magmas (56-59% SiO_2) according to Heicken (1974). We consider that these tephra layers are associated with the Calbuco volcano. At least 12

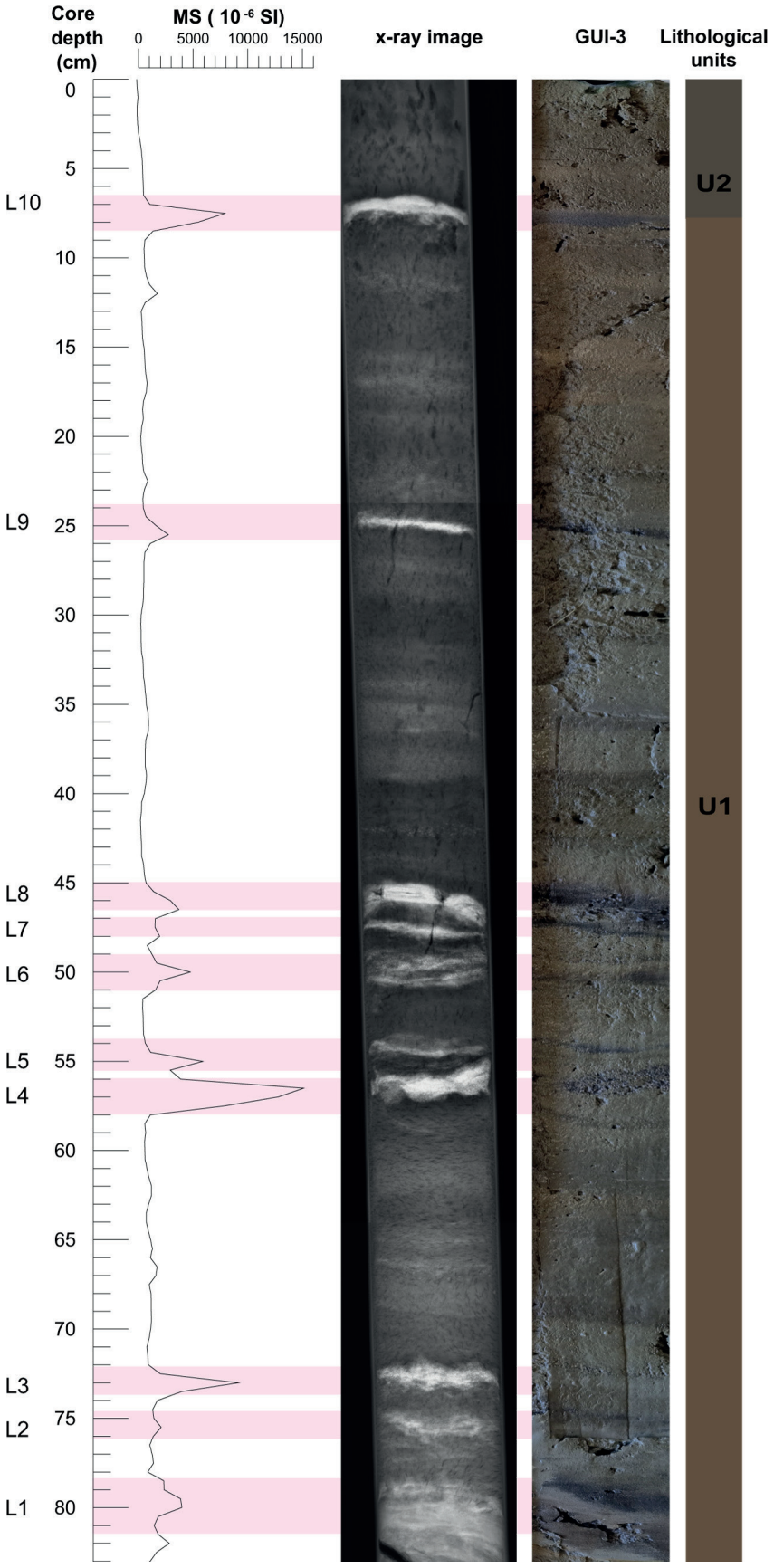

Figure 9. Magnetic susceptibility and X-ray image of GUI-3 core. The pink shadows indicate the intervals where the layers of interest are located.

historical eruptions of this volcanic center have been reported since 1792, three of them having a VEI ≥3 (Romero *et al.*, 2016). These deposits are composed of pumice, scoria, and glass shards with basaltic-andesite to andesitic composition (~52.5 to 58.5 wt% SiO_2) and subordinate free crystals (plagioclase feldspar, pyroxene, amphibole, and quartz) (Daga *et al.*, 2008, 2014; Castruccio *et al.*, 2016; Morgado Bravo, 2019; Romero *et al.*, 2021). We preliminary attribute these tephras to the Calbuco volcanic events documented for the surrounding area: L2 (76.4 - 75 cm depth) to the volcanic eruption of 1893-1895, L4 (≈ 56,5 cm depth) to the volcanic eruption of 1907-1906, (López-Escobar *et al.*, 1992; Petit-Breuilh, 1995; Daga *et al.*, 2008; Romero *et al.*, 2021; Global Volcanism Program, 2023); L5 (55.1 - 55 cm depth) to the volcanic eruption of 1909 (Romero *et al.*, 2021, Global Volcanism Program, 2023); L6 is associated with the event of 1911-1912 (Reichert, 1917; Petit-Breuilh, 1995; Romero *et al.*, 2021); L7 (48.3 - 48 cm depth) to the volcanic eruption of 1917 (Sellés and Moreno, 2011; Romero *et al.*, 2016 and 2021), L9 (25.7- 25.5 cm depth) to the volcanic event of 1945 according to Petit-Breuilh (1995 and references therein), and finally L10 (7.5 - 7.2 cm depth) is associated to the 1972 eruption (Petit-Breuilh, 1995; González-Ferrán, 1995; Romero *et al.*, 2021). This layer (L10) was correlated to L5 (GUI-1 and GUI-2, 10.2-9.8 and 9.5 – 8.5 cm depth, respectively) due to the similar petrographic contents.

The white, highly vesiculated pumice and obsidian fragments in L3 and L8 (GUI-3) are associated with rhyolitic magmas, according to Heicken (1974). Therefore, these tephra layers are consistent with the Cordón Caulle Volcanic Center. The last three eruptions (1921, 1960, and 2011) display similar magma compositions (Jay *et al.*, 2014). They were explosive, sub-plinian eruptions of ~1 km^3 of crystal-poor rhyodacitic magma (70-71% SiO_2) (Naranjo *et al.*, 2017). Its tephra deposits are described as mainly composed of whitish and highly vesiculated pumice with a few phenocrysts of plagioclase, two types of pyroxenes (ortho and clyno pyroxenes), and magnetite, sparsely distributed in the vesicular glass (Katsui and Katz, 1967; Collini *et al.*, 2013). We estimate that L3 (73.1 - 72.9 cm depth) could be associated with the 1893 eruption (Petit-Breuilh, 1995; Global Volcanism Program, 2023). Finally, L8 (46.5 - 45.9 cm depth) was associated with the volcanic eruption of 1921-1922 (Katsui and Katz, 1967; González-Ferrán, 1995; Lara *et al.*, 2004; Singer *et al.*, 2008, among others).

Identification of hyperpycnal flow events

The south region of Nahuel Huapi National Park has been affected by several natural disturbances during the last years, especially those associated with heavy rains and mass wasting phenomenon, both subaerial and subaqueous processes. According to Bates (1953), considering the relationship between the density of the river discharge (flow) and that of the receiving water body (lacustrine or marine basin), three main types of flows are differentiated shaping the different delta types: hypopycnal, homopycnal, and hyperpycnal flows. On freshwater lakes, hyperpycnal flows are very common since only 1 kg/m^3 of suspended sediment is required in the incoming flow to become hyperpycnal flow. A hyperpycnal flow occurs when the density of the incoming flow is higher than that of the water in the reservoir. The river mouth was historically considered the zone where most terrigenous sediments accumulate due to the drastic deceleration and loss of confinement of these stream flows when reaching the coast (Zavala *et al.*, 2018).

Though the cores were taken relatively near the coast of Lago Guillelmo, and could be affected by the presence of coastal processes (such as subaqueous landslides), we consider that the main source of the disturbance events identified in the sedimentary record of Lago Guillelmo is related to hyperpycnal flows that reach the lake. This interpretation is based on the normal grain size grading (from medium sand to very fine sand), presence of terrestrial plant debris, and coring site location close to the mouth of the rivers, far from the head scars associated with underwater landslides detected in the bathymetry. We interpret that several layers, especially from Cores GUI-1 and GUI-2, correspond to hyperpycnites. In particular, the location of the coring site of GUI-2 corresponds to the mouth of an abandoned river course, identified as C3. In GUI-3, we did not identify any discrete layer associated with hyperpycnal flows because this core is located several meters away from the mouth of the streams, in an environment with less energy. The correlation of the GPR profiles B-B' and C-C' with the sedimentary analysis of GUI-2 allowed us to suggest that the lobe morphology corresponds to this particular layer L1,

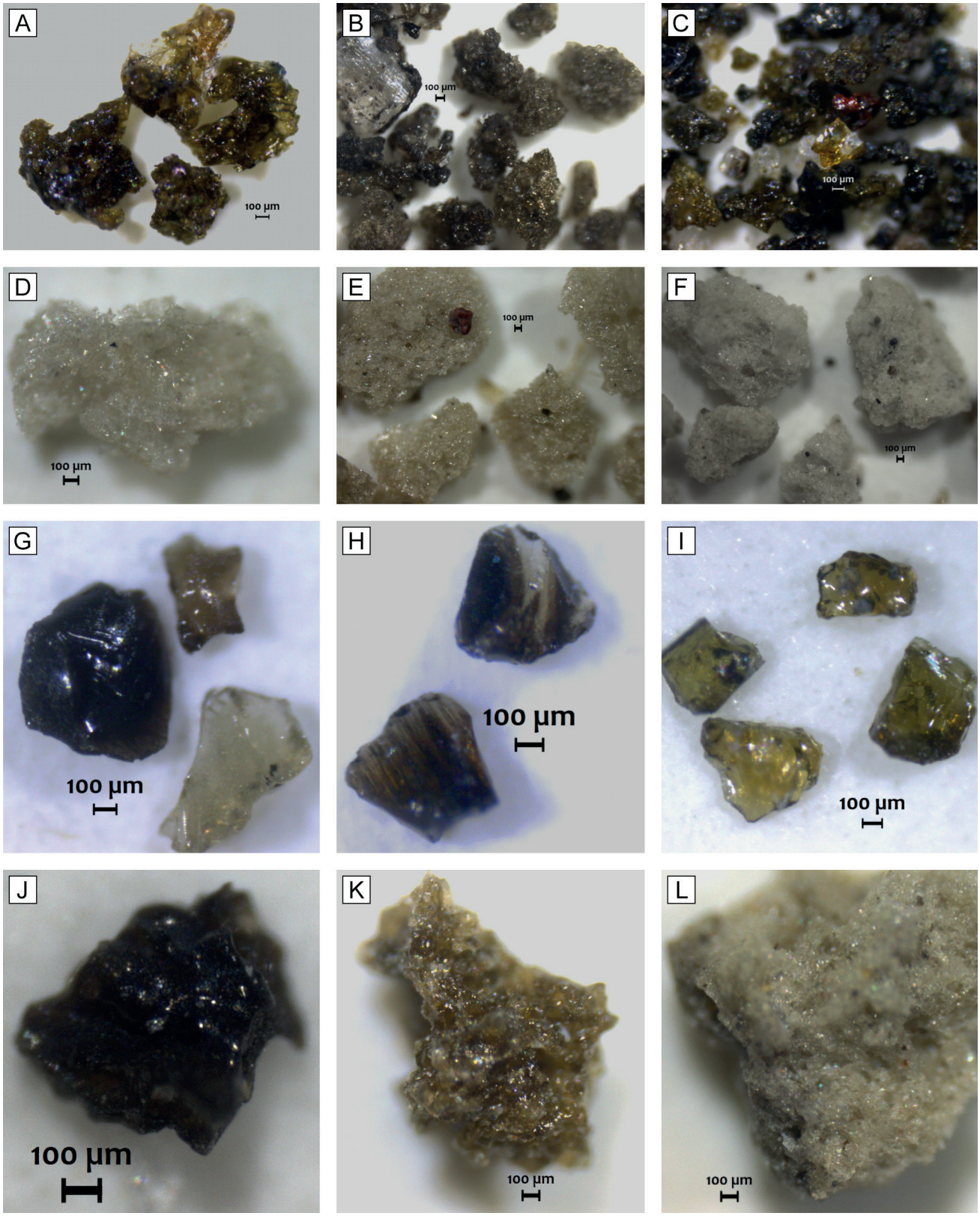

Figure 10. Different vitroclast populations identified in GUI-3 core. **a)** Broken droplets, **b)** and **c)** dark scoriaceous fragments identified in L1. **d), e)** and **f)** correspond to white pumiceous fragments highly vesiculated, identified in L3, L4 and L8. **g), h)** and **i)**: obsidian fragments identified also in L3 and L8. **j)**, dark scoriaceous fragments, **k)**: greenish pumiceous fragment **l)**: white pumiceous fragment with high vesicularity, identified In L4, L5, L6, L7, L9 and L10.

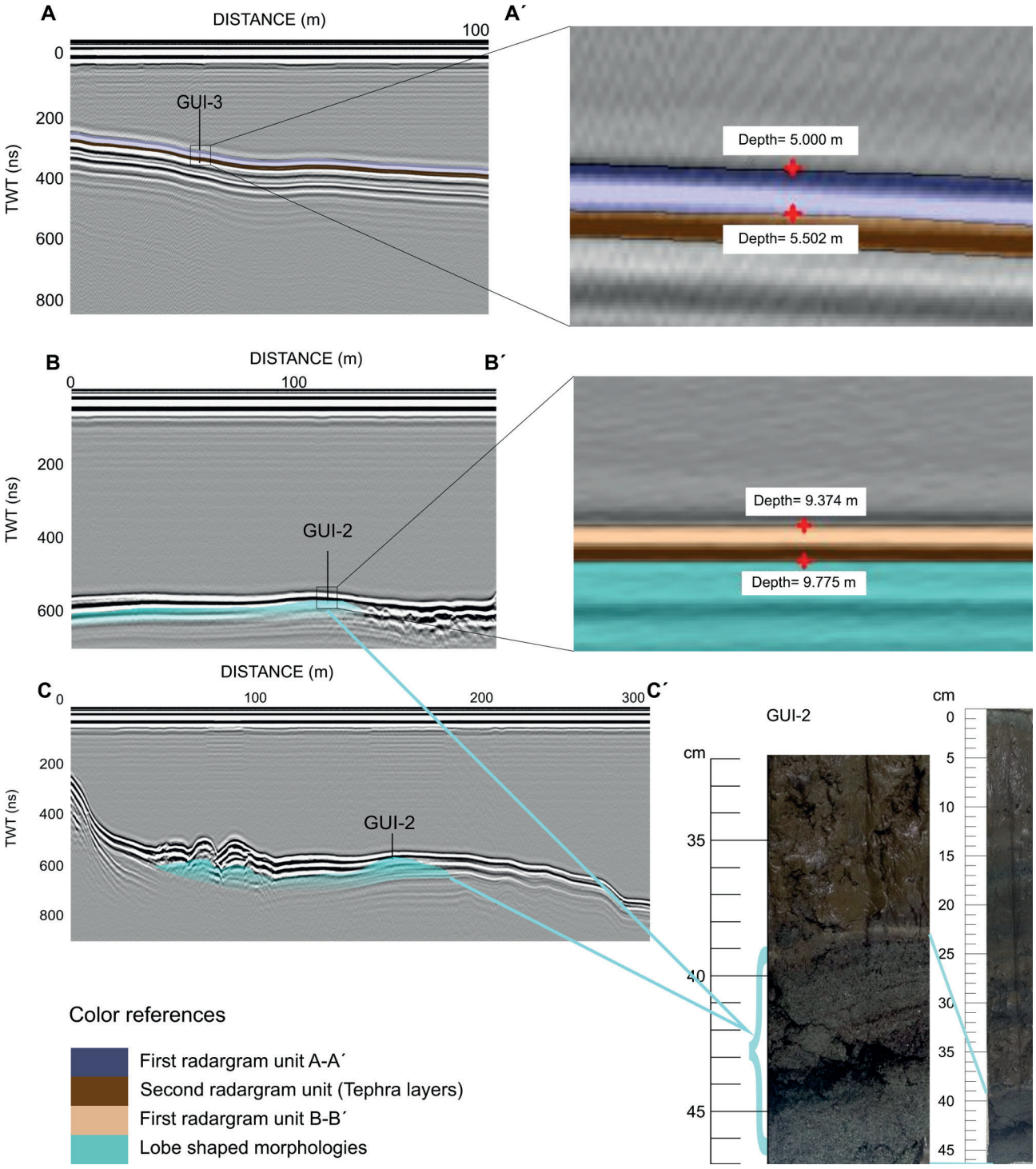

Figure 11. Interpreted GPR profiles across the Guillelmo Lake. For location, see Figure 3. Correspondence between L1 GUI-2 and the lobe shaped morphology that appears in radargrams.

associated with Unit 1 of GUI-2 (Fig. 11).

We interpret that the gravel mining in the delta imposed an obstacle to the sediment transport carried by flows that circulated through the southern sector of the delta, making it difficult for them to arrive the lake, generating topographic depressions that acted as sediment traps, as seen in the longitudinal profiles generated with GIS. This assumption is supported by a transition in sediment type from inorganic, laminated coarse silt and very fine sand

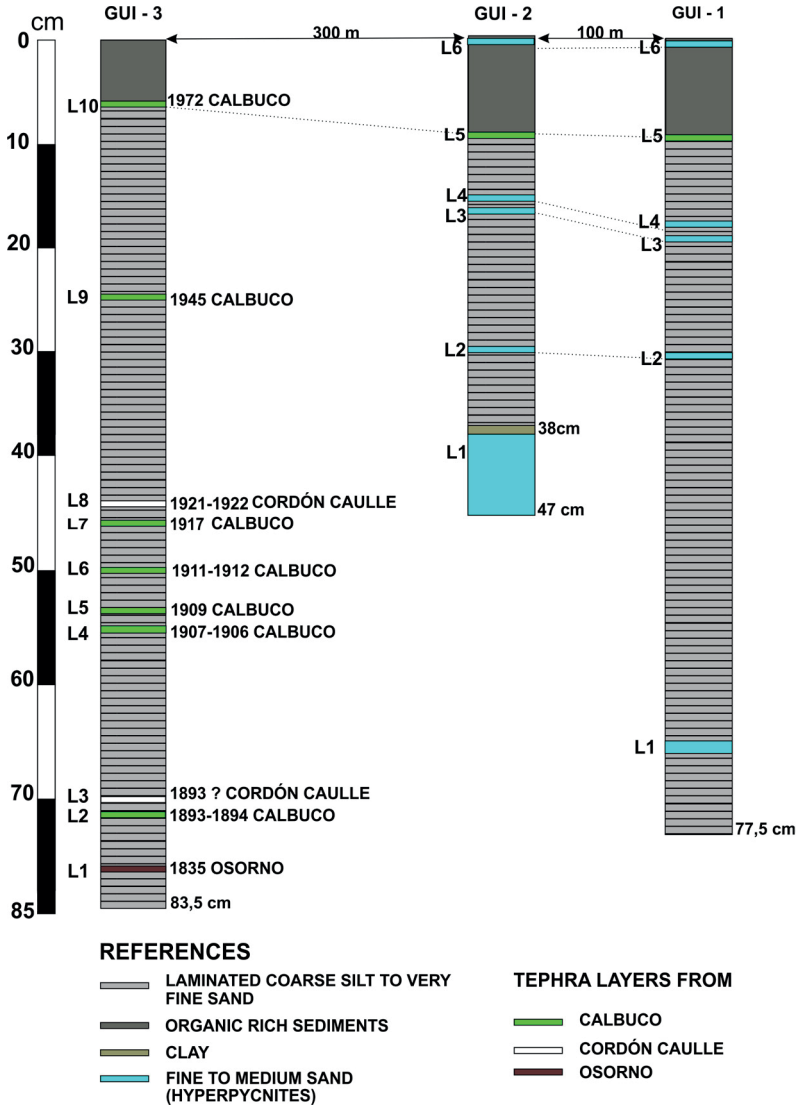

Figure 12. Correlation and interpretation of the three cores and their layers and associated events.

to organic-rich fine sediments observed in all cores. The lithological change to more organic sediments would correspond to a significant interruption/decrease in the epiclastic sediments input coming from the fluvial system, being represented almost exclusively by organic sedimentation derived from the productivity of the lake, after gravel mining settlement in the late 1970s.

At the top of GUI-1 and GUI-2, we identified a layer of epiclastic accumulation (L6 - 1-0.2 cm), also interpreted as a hyperpycnite. As described in the introduction, important debris flows occurred in the area in 2015. Mancini and Cordo (2023) mentioned that this debris flow crossed the route, generating major accumulations of sediments in the distal zone of the delta fan and gravel mining pits. Satellite images from before and after the event allowed us to confirm that this flow even reached the lake. Thus, we assume that L6 (from both GUI-1 and GUI-2) corresponds to the finest fraction of this debris flow, while the coarsest fraction was retained in the delta.

CONCLUSIONS

In Lago Guillelmo, the multi-approach evaluation based on land surface and subaqueous environment analysis allowed us to identify natural disturbances associated with heavy rains, such as hyperpycnal flows, and pyroclastic falls related to Osorno, Calbuco, and Cordon Caulle volcanoes.

In core GUI-3 we identified 10 tephra layers: L1, associated with the 1935 Osorno volcanic eruption; L2, L4, L6, L9, and L10 related to the Calbuco eruptions of 1893-1895, 1906-1907, 1909,

1911-1912, 1917, 1945, and 1972, respectively; and finally, L3 and L8 were correlated to the Cordón Caulle eruptions of 1893 and 1921-1922. We linked L3, L4, L5, and L6 with a radar unit identified at approximately 50 cm in A-A' GPR profile.

Five layers in cores GUI-1 and GU1-2 were interpreted as hyperpycnites (L1, L2, L3, L4 and L6). L6 (GUI1-GUI2) was linked to the February 2015 debris flow that caused road cuts and reached the lake. We also correlate L1 (GUI-2) with lobulated morphologies identified in B-B' and C-C' GPR profiles.

Finally, we interpret that the decrease of lamination at the top of the lacustrine sediments studied is related to anthropic activities, *i.e.*, the construction of Nacional Route 40 and the gravel mining that disturbed the distal network of the La Cantera watershed.

The results of this work demonstrate that lake sediments of Lago Guillelmo are capable of recording natural and anthropic disturbances proving the utility this system has to elaborate reconstructions, not only of adverse events related to these phenomena but also to make paleoclimatic inferences. This work will be extended to other watersheds of Northern Patagonia, linking land surface and subaqueous environment analysis.

Acknowledgments

This study was supported by the Agencia Nacional de Promoción Científica y Tecnológica (Argentina) (PICT 2016–0084 and PICT 2020-2245), CONICET (PIP 2020-2980) and the Universidad Nacional del Comahue (Argentina) (PIN I 04/B 226). The authors thank Agencia Nacional de Parques for allowing us to work in the Parque Nacional Nahuel Huapi. We also thank the guest editor Dr. Alfonsina Tripaldi, and Dr. Carina Colombi and an anonymous reviewer for the important suggestions that enhanced the present work. Finally, we thank Lic. Ana Luisa Figueira Sales for helping us to improve the English redaction.

REFERENCES

Alloway, B.V., Pearce, N.J.G., Villarosa, G., Outes, V., and Moreno, P.I. (2015). Multiple melt bodies fed the AD 2011 eruption of Puyehue-Cordón Caulle, Chile. *Scientific reports*, 5(1): 17589.

Alloway, B.V., Pearce, N.J., Moreno, P.I., Villarosa, G., Jara, I.A., Henríquez, C.A., and Outes, V. (2022). Refinement of the tephrostratigraphy straddling the northern Patagonian Andes (40–41° S): new tephra markers, reconciling different archives and ascertaining the timing of piedmont deglaciation. *Journal of Quaternary Science*, 37(3): 441-477.

Ariztegui, D., Bianchi, M.M., Masaferro, J., Lafargue, E., and Niessen, F. (1997). Interhemispheric synchrony of Late-glacial climatic instability as recorded in proglacial Lake Mascardi, Argentina. *Journal of Quaternary Science,* 12(4), 333-338.

Ariztegui, D., Anselmetti, F.S., Kelts, K., Seltzer, G.O., and D'Agostino, K. (2001). Identifying paleoenvironmental change across South and North America using high-resolution seismic stratigraphy in lakes. In: Markgraf, V. (Ed.), *Interhemispheric climate linkages*, pp. 227-240. Academic Press.

Ariztegui, D., Anselmetti, F.S., Gilli, A., and Waldmann, N. (2008). Late Pleistocene environmental change in Eastern Patagonia and Tierra del Fuego–A limnogeological approach. *Developments in Quaternary Sciences*, 11: 241-253.

Bariloche2000 (2015). https://www.bariloche2000.com/noticias/leer/cortan-el-transito-en-la-ruta-40-por-un-alud-en-el-lago-guillelmo/89252

Bates, C. (1953). Rational theory of delta formation. AAPG Bulletin, 37: 2119-2162.

Beigt, D., Villarosa, G., Outes, A.V., Dzendoletas, M.A., and Gomez, E.A. (2013). Tsunamis en el lago Nahuel Huapi: historias de deslizamientos y erupciones. *Desde La Patagonia Difundiendo Saberes,* 10: 10-15.

Beigt, D., Villarosa, G., and Gomez, E.A. (2014). Análisis de deslizamientos subacuáticos en deltas lacustres (Nahuel Huapi, Argentina) a partir de batimetrías de alta resolución. *Cuadernos de Investigación Geográfica*: 247-259.

Beigt, D., Villarosa, G., Gómez, E.A., and Manzoni, C. (2016). Subaqueous landslides at the distal basin of Lago Nahuel Huapi (Argentina): Towards a tsunami hazard evaluation in Northern Patagonian lakes. *Geomorphology*, 268: 197-206.

Beigt, D., Villarosa, G., De Luca, L., Barbosa Hetherington, A., Gómez, E.A., Raniolo, A. (2023). Inestabilidad de costas asociada a fenómenos gravitacionales en grandes lagos patagónicos: un análisis de eventos recientes. *Revista de la Asociación Geológica Argentina*. (In press).

Bengtsson, L., and Enell, M., (1986). Chemical analysis. In: Berglund, B.E. (Ed.), *Handbook of Palaeoecology and Palaeohydrology*, John Wiley and Sons, p. 423-451.

Bertrand, S., Castiaux, J., and Juvigné, E. (2008). Tephrostratigraphy of the late glacial and Holocene sediments of Puyehue Lake (southern volcanic zone, Chile, 40 S). *Quaternary Research*, 70(3): 343-357.

Bertrand, S., Daga, R., Bedert, R., and Fontijn, K. (2014). Deposition of the 2011–2012 Cordón Caulle tephra (Chile, 40 S) in lake sediments: Implications for tephrochronology and volcanology. *Journal of Geophysical Research: Earth Surface*, 119(12): 2555-2573.

Cabrera, A.L. (1976). Regiones fitogeográficas argentinas. *Enciclopedia argentina de agricultura y jardinería*, 2*:* 1-85.

Castruccio, A., Clavero, J., Segura, A., Samaniego, P., Roche, O., Le Pennec, J.L., and Droguett, B. (2016). Eruptive parameters and dynamics of the April 2015 sub-Plinian eruptions of Calbuco volcano (southern Chile). *Bulletin of Volcanology*, 78*:* 1-19.

Chanu, S.R., Chingkhei, R.K., Sanoujam, M., and Kumar, A. (2014). Lake sediment thickness estimation using Ground Penetrating Radar. *International Journal of Research in Engineering and Technology*, 3*:* 42.

Chapron, E., Ariztegui, D., Mulsow, S., Villarosa, G., Pino, M., Outes, V., and Crivelli, E. (2006). Impact of the 1960

major subduction earthquake in Northern Patagonia (Chile, Argentina). *Quaternary International*, 158(1): 58-71.

Chapron, E., Juvigné, E., Mulsow, S., Ariztegui, D., Magand, O., Bertrand, S., Pino, M. and Chapron, O. (2007). Recent clastic sedimentation processes in Lake Puyehue (Chilean Lake District, 40.5 S). *Sedimentary Geology*, 201(3-4): 365-385.

Collini, E., Osores, M.S., Folch, A., Viramonte, J.G., Villarosa, G., and Salmuni, G. (2013). Volcanic ash forecast during the June 2011 Cordón Caulle eruption. *Natural hazards*, 66*:* 389-412.

Cotelo, M.A. (2019). *Análisis de riesgo por eventos de remoción en masa, propuesta de Plan de Mitigación. Ruta Nacional 40 sur, Lago Guillelmo, Departamento Bariloche* (Doctoral dissertation, Unpublished).

Daga, R., Guevara, S.R., Sánchez, M.L., and Arribére, M. (2008). Source identification of volcanic ashes by geochemical analysis of well preserved lacustrine tephras in Nahuel Huapi National Park. *Applied Radiation and Isotopes*, 66(10): 1325-1336.

Daga, R., Guevara, S.R., Poire, D.G., and Arribére, M. (2014). Characterization of tephras dispersed by the recent eruptions of volcanoes Calbuco (1961), Chaitén (2008) and Cordón Caulle Complex (1960 and 2011), in Northern Patagonia. *Journal of South American Earth Sciences*, 49: 1-14.

De Fontaine, C.S., Kaufman, D.S., Anderson, R.S., Werner, A., Waythomas, C.F., and Brown, T.A. (2007). Late Quaternary distal tephra-fall deposits in lacustrine sediments, Kenai Peninsula, Alaska. *Quaternary Research*, 68(1): 64-78.

Del Valle, R.A., Lirio, J.M., Nunez, H.J., Tatur, A., and Rinaldi, C.A. (2000). Sedimentary cores from Mascardi Lake, Argentina: a key site to study Elpalafquen paleolake. In: Smolka, P. and Volkheimer, W. (Eds.), *Southern Hemisphere Paleo-and Neoclimates: Key Sites, Methods, Data and Models:* 275-286.

Deng, Y.N., Rioual, P., Jones, V.J., Sun, C., and Mingram, J. (2023). A palaeoecological study investigating the impacts of multiple tephra depositions on a lacustrine ecosystem in Northeast China, using diatoms as environmental indicators. *Journal of Paleolimnology*, 70(1): 1-22.

El Cordillerano (2013). https://www.elcordillerano.com.ar/noticias/2013/09/08/8580-ruta-a-el-bolson-cortada-por-alud-de-barro

Fisher, R.V., and Schmincke, H.U. (2012). *Pyroclastic rocks*. Springer Science and Business Media, 472 p.

Flint, R.F., and Fidalgo, F. (1964). Glacial geology of the East flank of the Argentine Andes between -Latitude 39 10′ S. and Latitude 41 20′ S. *Geological Society of America Bulletin*, 75(4): 335-352

Fontijn, K., Lachowycz, S.M., Rawson, H., Pyle, D.M., Mather, T.A., Naranjo, J.A., and Moreno-Roa, H. (2014). Late Quaternary tephrostratigraphy of southern Chile and Argentina. *Quaternary Science Reviews*, 89: 70-84.

Fontijn, K., Rawson, H., Van Daele, M., Moernaut, J., Abarzúa, A.M., Heirman, K., Bertrand, S., Pyle, D.M., Mather, T.A., De Batist, M., Naranjo, J.A., and Moreno, H. (2016). Synchronisation of sedimentary records using tephra: A postglacial tephrochronological model for the Chilean Lake District. *Quaternary Science Reviews*, 137*:* 234-254.

Giacosa, R.E., Heredia Carballo, N., Zubía, M.A., González, R., Faroux, A.J., Césari, O., and Franchi, M. 2001. *Hoja Geológica 4172-IV San Carlos de Bariloche*. Instituto de Geología y Recursos Minerales, Servicio Geológico Minero Argentino. Boletín 279, 77 p. Buenos Aires.

Giardino, C., Oggioni, A., Bresciani, M., and Yan, H. (2010). Remote sensing of suspended particulate matter in Himalayan lakes. *Mountain Research and Development*, 30(2): 157-168.

Global Volcanism Program, (2023). [DatabaGlobal Volcanism Program, 2023. [Database] Volcanoes of the World (v. 5.0.2; 23 Jan 2023). Distributed by Smithsonian Institution, compiled by Venzke, Ese.

González-Ferrán, O. (1995). *Volcanes de Chile*. Instituto Geográfico Militar, 640 p, Santiago de Chile.

Gordon, A. and Ort, M.H. (1993). *Edad y correlación del plutonismo subcordillerano en las provincias de Río Negro y Chubut (41°-42°30'L.S)*. Congreso Geológico Argentino, No. 12, Actas 4: 120-127. Mendoza.

Gorelick, N., Hancher, M., Dixon, M., Ilyushchenko, S., Thau, D., and Moore, R. (2017). Google Earth Engine: Planetary-scale geospatial analysis for everyone. *Remote sensing of Environment*, 202: 18-27.

Guilizzoni, P., Massaferro, J., Lami, A., Piovano, E.L., Guevara, S.R., Formica, S.M., Daga, R., Rizzo, A., and Gerli, S. (2009). Palaeolimnology of Lake Hess (Patagonia, Argentina): Multi-proxy analyses of short sediment cores. *Hydrobiologia,* 631: 289-302.

Heiken, G. (1974). Atlas of volcanic ash. *Smithsonian Contributions to the Earth Sciences*, 101 p.

Heiri, O., Lotter, A. F., and Lemcke, G. (2001). Loss on ignition as a method for estimating organic and carbonate content in sediments: reproducibility and comparability of results. *Journal of paleolimnology*, 25: 101-110.

Iglesias, V., Whitlock, C., Bianchi, M.M., Villarosa, G., and Outes, V. (2012). Climate and local controls of long-term vegetation dynamics in northern Patagonia (Lat 41 S). *Quaternary Research*, 78(3): 502-512.

Iglesias, V., and Whitlock, C. (2014). Fire responses to postglacial climate change and human impact in northern Patagonia (41–43 S). *Proceedings of the National Academy of Sciences*, 111(51): E5545-E5554.

Katsui, Y., and Katz, H.R. (1967). Lateral fissure eruptions in the southern Andes of Chile. *Journal of the Faculty of Science, Hokkaido University. Series 4, Geology and mineralogy*, 13(4): 433-448.

La Nación (2014). https://www.lanacion.com.ar/sociedad/parte-de-la-ruta-40-cortada-tras-un-alud-de-barro-y-piedras-en-bariloche-nid1715219/

Lara, L.E., Moreno, H., Naranjo, J.A., Matthews, S., and De Arce, C.P. (2006). Magmatic evolution of the Puyehue–Cordón Caulle Volcanic Complex (40 S), Southern Andean Volcanic Zone: from shield to unusual rhyolitic fissure volcanism. *Journal of Volcanology and Geothermal Research*, 157(4): 343-366.

Lara, L.E., Naranjo, J.A., and Moreno, H. (2004). Rhyodacitic fissure eruption in Southern Andes (Cordón Caulle; 40.5 S) after the 1960 (Mw: 9.5) Chilean earthquake: a structural interpretation. *Journal of Volcanology and Geothermal Research*, 138(1-2): 127-138.

Lara, L.E., Orozco, G., and Piña-Gauthier, M. (2012). The 1835 AD fissure eruption at Osorno volcano, Southern Andes: Tectonic control by the intraarc stress field instead of remote megathrust-related dynamic strain. *Tectonophysics*, 530: 102-110.

Lopez-Escobar, L., Parada, M.A., Moreno, H., Frey, F.A., and Hickey-Vargas, R.L. (1992). A contribution to the petrogenesis of Osomo and Calbuco volcanoes, Southern Andes (41° 00'-41° 30'S): comparative study. *Andean Geology*, 19(2): 211-226.

Mancini, P.G., and Cordo, O.V. (2023). Propuestas de control de acarreos en Ruta Nacional 40. Lago Guillelmo-Bariloche: Debris control proposals on National Route 40. Lake Guillelmo-Bariloche. *Infraestructura Vial*, 25(44): 1-10.

Maruddani, B., and Sandi, E. (2019). The development of ground penetrating radar (GPR) data processing. *International Journal of Machine Learning and Computing*, 9: 768-773.

Matta, E., Giardino, C., Boggero, A., and Bresciani, M. (2017). Use of satellite and in situ reflectance data for lake water color characterization in the Everest Himalayan region. *Mountain research and development*, 37(1): 16-23.

Mermoz, M., Kitzberger, T., and Veblen, T.T. (2005). Landscape influences on occurrence and spread of wildfires in Patagonian forests and shrublands. *Ecology*, 86(10): 2705-2715.

Mizerit, I. (2017). *Evaluación de la susceptibilidad a procesos de remoción en masa en los alrededores de los lagos Mascardi y Guillelmo, Parque Nacional Nahuel Huapi, Río Negro*. Ph.D. dissertation (Unpublished).

Morgado Bravo, E.E. (2019). *Pre-eruptive conditions, crustal processes, and magmatic timescales recorded in products of Calbuco and Osorno volcanoes, Southern Andes*. Ph.D. dissertation, University of Leeds (Unpublished).

Mulder, T., Syvitski, J.P., Migeon, S., Faugères, J. C., and Savoye, B. (2003). Marine hyperpycnal flows: initiation, behavior and related deposits. A review. *Marine and Petroleum Geology*, 20(6-8): 861-882.

Naranjo, J.A., Singer, B.S., Jicha, B.R., Moreno, H., and Lara, L.E. (2017). Holocene tephra succession of Puyehue-Cordón Caulle and Antillanca/Casablanca volcanic complexes, southern Andes (40–41 S). *Journal of Volcanology and Geothermal Research*, 332*:* 109-128.

New, M., Lister, D., Hulme, M., and Makin, I. (2002). A high-resolution data set of surface climate over global land areas. *Climate research*, 21(1): 1-25.

Paruelo, J.M., Beltrán, A., Jobbágy, E., Sala, O.E., and Golluscio, R.A. (1998). The climate of Patagonia: general patterns and controls on biotic processes. *Ecología austral*, 8(02): 85-101

Pereyra F., Elissondo M., López C., Dzendoletas A., Roverano D. y Wilson C. (2009). *Carta de Peligrosidad Geológica 4172-IV San Carlos de Bariloche*. Servicio Geológico Minero Argentino. Programa Nacional de Cartas Geológicas de la República Argentina. Dirección de Geología Ambiental y Aplicada. Boletín N° 390.

Perez, L., Castruccio, A., and Diaz, D. (2019). *Eruptive dynamics of the 1835 Osorno volcano flank eruption, Chile (41° S)*. AGU Fall Meeting Abstracts: pp. V23F-0268.

Petit-Breuilh, S. (1995). *Evaluación del impacto de erupciones históricas en algunos volcanes de alto riesgo de los Andes del Sur: Nevados de Chillán, Cordón Caulle, Osorno, Calbuco y Hudson, Chile*. Informe final. Temuco, Chile, 98 p.

Petit-Breuilh, M.E. (1999). *Cronología Eruptiva Histórica de los volcanes Osorno y Calbuco*. Servicio Nacional de Geología y Minería, Boletín No. 53, 45p. Santiago.

Quirós, R. (1988). *Mapas batimétricos y parámetros morfométricos de lagos patagónicos de Neuquén, de Río Negro y del Chubut (Argentina)*. Instituto Nacional de Investigación y Desarrollo Pesquero. Informe Técnico Nº 5.

Rabassa, J., and Coronato, A. (2009). Glaciations in Patagonia and Tierra del Fuego during the Ensenadan stage/age (early Pleistocene–earliest middle Pleistocene). *Quaternary International*, 210(1-2), 18-36.

Reichert, F. (1917). Las regiones inexploradas o poco conocidas de la cordillera norpatagónica. *Sociedad Científica Alemana: Santiago, Chile*, 119 p.

Reynolds, J.M. (2011). *An introduction to applied and environmental geophysics*. John Wiley and Sons, p. 539 - 551.

Romero, J.E., Alloway, B.V., Gutiérrez, R., Bertín, D., Castruccio, A., Villarosa, G., Schipper, C.I., Guevara, A., Bustillos, J., Pisello, A., Daga, R., Monitel, M., Gleeman, E., González, M., Morgavi, D., Ribeiro Guevara, S. and Mella, M. (2021). Centennial-scale eruptive diversity at Volcán Calbuco (41.3° S; Northwest Patagonia) deduced from historic tephra cover-bed and dendrochronologic archives. *Journal of Volcanology and Geothermal Research*, 417*:* 107281

Romero, J.E., Morgavi, D., Arzilli, F., Daga, R., Caselli, A., Reckziegel, F., Perugini, D. (2016). Eruption dynamics of the 22–23 April 2015 Calbuco Volcano (Southern Chile): Analyses of tephra fall deposits. *Journal of Volcanology and Geothermal Research*: 317, 15-29.

Selles, D., and Moreno, H. (2011). *Geología del volcán Calbuco, Región de Los Lagos*. Servicio Nacional de Geología y Minería, Carta Geológica de Chile, Serie Geología Básica 130: 38 p., 1 mapa escala 1: 50.000. *Santiago*.

Singer, B.S., Jicha, B.R., Harper, M.A., Naranjo, J.A., Lara, L.E., and Moreno-Roa, H. (2008). Eruptive history, geochronology, and magmatic evolution of the Puyehue-Cordón Caulle volcanic complex, Chile. *Geological Society of America Bulletin*, 120(5-6): 599-618.

Soulié-Märsche, I., and García, A. (2015). Gyrogonites and oospores, complementary viewpoints to improve the study of the charophytes (Charales). *Aquatic Botany*, 120: 7-17.

Steen-McIntyre, V. (1977). *A man ual for tephrochronology: Collection, preparation, petrographic description and approximate dating of tephra (volcanic ash)*. Steen-McIntyre, 167 p.

Pickett, S.T.A. and White, P.S. (1985) *The Ecology of Natural Disturbance and Patch Dynamics*. Academic Press, Orlando. 472 p.